

ab initio Study of Strain-Induced Ferroelectricity in SrTiO₃

Takatoshi HASHIMOTO^{1,2}*, Takeshi NISHIMATSU¹,
Hiroshi MIZUSEKI¹, Yoshiyuki KAWAZOE¹,
Atsushi SASAKI², and Yoshiaki IKEDA²

¹Institute for Materials Research (IMR),
Tohoku University, Sendai 980-8577, Japan
²NEC TOKIN Corporation, Sendai 982-8510, Japan

March 23, 2022

Abstract

Valley lines on total-energy surfaces for the zone-center distortions of free-standing and in-plane strained SrTiO₃ are investigated with a newly developed first-principles structure optimization technique [Jpn. J. Appl. Phys. **43** (2004), 6785]. The results of numerical calculations confirmed that the ferroelectricity is induced, and the Curie temperature is increased, by applying biaxial compressive or tensile strains. Along the distortion, strong nonlinear coupling between the soft- and hard-modes is demonstrated.

Keywords

density functional theory, local density approximation, biaxial strain, potential surface, Slater mode, Last mode

1 Introduction

Perovskite structure strontium titanate, SrTiO₃, is an extremely important material. Because of its wide range of physical properties, such as semiconductivity, superconductivity, incipient ferroelectricity and catalytic activity, SrTiO₃ is expected to be used for a variety of technological applications. Bulk SrTiO₃ crystallizes in the cubic centrosymmetric (O_h^1) structure, and is paraelectric at room temperature. Atomic fractional coordinates are Sr(0,0,0), Ti($\frac{1}{2}$, $\frac{1}{2}$, $\frac{1}{2}$), O_I(0, $\frac{1}{2}$, $\frac{1}{2}$), O_{II}($\frac{1}{2}$, 0, $\frac{1}{2}$), and O_{III}($\frac{1}{2}$, $\frac{1}{2}$, 0) respectively, as depicted in Fig. 1. SrTiO₃'s tolerance factor [1], calculated with Shannons's ionic radii [2], is $t = 1.002$. This almost unity value suggests that the cubic structure is moderately stable. Below 105K, SrTiO₃ undergoes a structural phase transition from

*Corresponding author. E-mail address: hasitaka@imr.edu

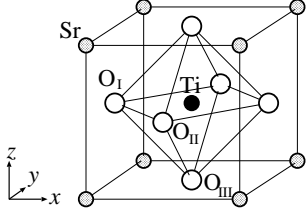


Figure 1: Cubic (O_h^1) crystal structure of perovskite oxide SrTiO_3 .

cubic to an antiferrodistortive (AFD) tetragonal (D_{4h}^{18}) structure, which is associated with zone-boundary phonon condensation at the R point. [3, 4, 5, 6, 7] This transition is driven by TiO_6 octahedral rotational mode instabilities; the rotation angle is less than 2° [8]. At lower temperatures, the dielectric constant exhibits Curie-Weiss law like behavior, but does not exhibit divergence. The dielectric constant saturates to a value of $\sim 2 \times 10^4$ under 10 K [9, 10], but no transition, e.g. to a ferroelectric state, actually occurs with decreasing temperature. Because of its failure to exhibit a ferroelectric phase transition, SrTiO_3 is generally regarded as an incipient ferroelectric, in which quantum fluctuations suppress ferroelectricity. The observed temperature dependence of SrTiO_3 's dielectric constant is well described by Barrett's formula[11],

$$\varepsilon = \frac{M}{\frac{1}{2}T_1 \coth\left(\frac{T_1}{2T}\right) - T_0}, \quad (1)$$

where T_0 is the *transition* temperature, T_1 is a characteristic dividing point below which quantum effects are important, and M is a constant. In ref. [12], these values for SrTiO_3 were given as $T_0 = 38$ K, $T_1 = 84$ K, and $M = 9 \times 10^4$ K, respectively. Thus, it had been long expected that SrTiO_3 would have ferroelectricity under some stresses or strains.

In recent years, the preparation of oxide thin films by thermal non-equilibrium techniques such as molecular beam epitaxy (MBE) and pulsed laser deposition (PLD), have enabled the growth of hetero-epitaxial thin films, and have attracted a great deal of attention. In 2004, J. H. Haeni *et al.* demonstrated that thin films of SrTiO_3 are ferroelectric near room temperature. [13] Using MBE, they grew SrTiO_3 thin films on a DyScO_3 substrate, to induce a biaxial tensile strain of the order of 1%, and measured the temperature dependence of the in-plane dielectric constant. Their results indicate that the nonpolar ground state of SrTiO_3 can be drastically transformed, to a polar state, by the application of small strains.

Ab initio calculations are attractive for atomistically analyzing the effects of structural distortions on properties such as Curie temperature. T. Schimizu studied the frequencies of Γ transverse-optical phonons in the cubic SrTiO_3 using the frozen-phonon scheme, and found that the dielectric constant strongly depends on strain at finite temperature [14]. A. Antons *et al.* have confirmed that the dielectric constant of SrTiO_3 epitaxial thin films varies significantly with strain using density functional theory (DFT) within the local-density approximation (LDA) [15]. However, the mechanism by which in-plane biaxial

strain induces ferroelectricity in SrTiO₃ has not been clarified. We investigate the relationship between SrTiO₃-ferroelectricity and in-plane biaxial strains, compressive and tensile, by analyzing valley lines of total-energy surfaces with *ab initio* structure optimization technique that we had developed [16]. Compared to the conventional soft-mode-only structure optimization technique, our approach has the advantages that it can: (1) accurately estimate total energy as a function of the amplitude of atomic displacements, (2) correctly investigate nonlinear coupling between soft-mode atomic displacements, hard-mode displacements, and lattice deformations.

In the next section, we briefly explain our structure optimization technique and the numerical methods used in this study. Results of calculations are shown in §3. In §4, we summarize the paper.

2 Method

2.1 structure optimization technique

To investigate the total-energy surfaces of perovskite oxides, we improve King-Smith and Vanderbilt's scheme [17] and redefine the amplitude of atomic displacements u_α as

$$u_\alpha = \sqrt{(v_\alpha^A)^2 + (v_\alpha^B)^2 + (v_\alpha^{O_I})^2 + (v_\alpha^{O_{II}})^2 + (v_\alpha^{O_{III}})^2}, \quad (2)$$

where v_α^τ is the displacement of each atom τ ($= A, B, O_I, O_{II}, O_{III}$) in the Cartesian directions of α ($=x, y, z$) from the symmetric perovskite structure (O_h^1 or D_{4h}^1). The total energy is evaluated as a function of $u = \sqrt{u_x^2 + u_y^2 + u_z^2}$ under the condition that v_α^τ and the strain components η_i ($i = 1, \dots, 6$; Voigt notation) minimize the total energy for each u using an *ab initio* norm-conserving pseudopotential method and geometric optimization. To simulate D_{4h}^1 epitaxial SrTiO₃ thin films, as illustrated in Fig. 2(a), under a substrate induced biaxial in-plane strain, only the c axis (i.e., η_3) is permitted to relax but other parameters $a = b$, $\alpha = \beta = \gamma = 90^\circ$ (i.e., $\eta_1, \eta_2, \eta_4, \eta_5$, and η_6) are fixed for all directions of polarizations, [001] (Fig. 2(b)), [110] (Fig. 2(c)), and [100] (Fig. 2(d)), to satisfy symmetry constraints. Total energy minimization under the constant- u_α constraint (i.e., on the sphere surface with a radius u_α) is performed iteratively. Fully detailed formalism of this structure optimization technique is given in ref. [16]. We continue iterative optimization of atomic and lattice structure until differences in total energies remain less than 10^{-7} Hartree for two successive iterations.

2.2 Calculation Methods

For all *ab initio* calculations, we use the ABINIT package [18] with adapting it for our structure optimization technique in its source code of Src_9drive/brdmin.f. Bloch wave functions of electrons are expanded into plane waves with a energy cutoff of 40 Hartree, using Teter's extended norm-conserving pseudopotentials. [19] To retain a constant energy cutoff and to avoid nonphysical discontinuities of total energies as function of volumes, a correction

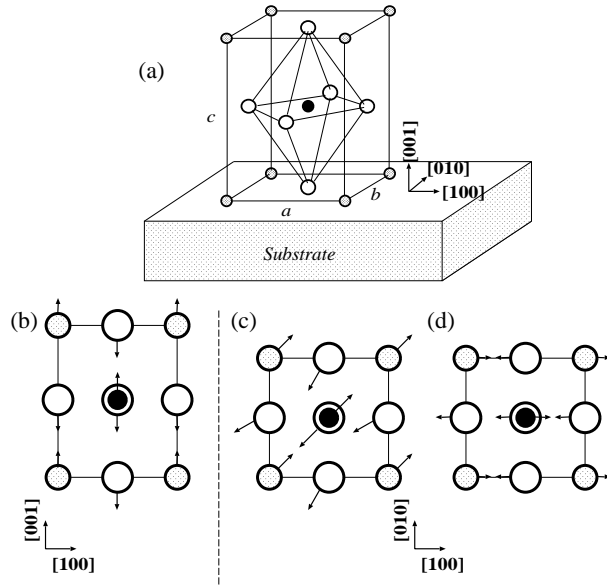


Figure 2: (a) Exaggerated illustration of epitaxially grown SrTiO₃ on substrate. Lattice constants a , $b(=a)$, and c and crystallographic directions $[100]$, $[010]$, and $[001]$ are indicated. (b) Pattern of atomic displacements accompanying $[001]$ tetragonal distortion under biaxial compressive strain is indicated by arrows in $(0\bar{1}0)$ projection. (c) That of $[110]$ monoclinic distortion under biaxial tensile strain in (100) projection. (d) That of $[100]$ monoclinic distortion under biaxial tensile strain in (100) projection.

of kinetic energies of plane waves just below the energy cutoff is introduced [20] as implemented in the ABINIT. This “energy cutoff smearing” technique is efficient not only for constant-pressure molecular dynamics but also for comparing total energies in different volumes. With this technique, one does not have to achieve convergence between constant-number-of-plane-waves calculations and constant-energy-cutoff calculations with respect to the basis set and, therefore, does not have to adopt a superfluously large energy cutoff. The pseudopotentials include O 2s and 2p, Ti 3s, 3p, 3d and 4s, Sr 4s, 4p and 5s, as valence electrons. Bloch wave functions are sampled on an $8 \times 8 \times 8$ grid of k -points in the first Brillouin zone. The exchange-correlation energy is treated within the local density approximation (LDA). As the parametrized correlation energy, we use Teter’s rational polynomial parameterization, [21] which reproduces the results obtained by Ceperley and Alder. [22] The electronic states are calculated by the iterative scheme to reach a tolerance of convergence that requires differences of forces to be less than 5×10^{-7} Hartree/Bohr for two successive iterations.

With these calculation methods, the calculated equilibrium lattice constant for cubic SrTiO₃ is 7.27 Bohr, which is $\sim 1.3\%$ less than the experimental value of 7.36 Bohr obtained by linearly extrapolating the lattice constant at high temperature to zero temperature (see Fig. 1 in ref. [23]). This underestimation is commonly considered to be a result of errors from LDA. Properties of ferroelectrics, especially total-energy surfaces, are very sensitive to the lattice constant [24]. Semi-empirical constraints on lattice constants in calculations of perovskite oxides have been commonly used to acquire agreements between the experimentally observed values and calculated results. Although artificial constraints can be introduced in our structure optimization technique, we do not employ such semi-empirical constraints. Nevertheless, we believe that calculations using LDA clarify some trends of displacive transitions in strained SrTiO₃.

The Berry-phase method [25, 26] is used to evaluate spontaneous polarizations.

For simplicity and to emphasize the origin of ferroelectricity in strained SrTiO₃, we neglect the AFD instabilities and use a single unit cell to calculate total-energy surfaces. We believe that this is a reasonable approximation because the effect of AFD on dielectric response is negligibly small. [27]

3 Results and Discussion

3.1 Free-standing SrTiO₃

Before examining in-plane strained SrTiO₃, we evaluated the total-energy surface of free-standing SrTiO₃ that is distorted from cubic to tetragonal and has [001] polarization. Shown in Fig. 3(a) is the total energy as a function of the amplitude of atomic displacements u_z . M. Itoh *et al.* found that ferroelectricity was induced in SrTiO₃ by the isotope exchange of ¹⁸O for ¹⁶O. [10] This isotope exchange experiment and the incipient ferroelectricity with $T_0 = 38$ K > 0 in Barrett’s formula suggest that the total energy *vs* u_z curve might have double well structure, but our calculated result does not. This is not just an artifact of the sensitivity of LDA total-energy surfaces to lattice constants, as described in refs. [24] and [28], rather, as we show in next subsection §3.2, the system is *very*

close to having a double well.

Calculated lattice constants a and c are well fitted by quadratic functions in Fig. 3(b). It is surprising that the amplitude of Sr-displacement, v_z^{Sr} , is smaller than that of Ti, v_z^{Ti} , for the soft-mode eigenvector calculated by the frozen phonon method at $u_z = 0$, but v_z^{Sr} becomes larger than v_z^{Ti} for $u_z > 0.07$ as shown in Fig. 3(c) and (d).

3.2 Effects of in-plane strains on SrTiO₃

Total energies of SrTiO₃ as functions of the amplitude of atomic displacements u are calculated for the tetragonal [001] distortion under in-plane biaxial compressive strains (Fig. 4(a)) and the monoclinic [110] (Fig. 4(b)) and [100] (Fig. 4(c)) distortions under in-plane biaxial tensile strains. It is confirmed that, for the biaxial tensile strained SrTiO₃, the [110] direction of ferroelectric polar distortion is energetically more preferable than that of [100] as compared in Fig. 5. Energy gain, the difference between total energy at $u = 0$ and its minimum value, grows up according to both compressive and tensile biaxial strains, though it is zero in the zero-strain $a = a_0$ case. The value of u , at which the system exhibits minimum total energy and equilibrium structure, also grows up according to the biaxial strains. In Fig. 6, we show calculated spontaneous polarizations for the equilibrium structures under biaxial strains $a = 0.95a_0 \sim 1.05a_0$. Under the compressive strain, spontaneous polarization appears above 1% and increases linearly as a function of strain. Under the tensile strain, spontaneous polarization appears a little below 1% and increases more gradually with strain. These calculated results represent that the transition temperature and the spontaneous polarization for ferroelectric ordering are predicted to be monotonically increasing functions of biaxial in-plane strains. In our calculated results, the energy gain becomes barely the order of room temperature ($300\text{ K} \approx 26\text{ meV}$) at 4% of compressive or tensile strains. The 4% of compressive or tensile strains are impractical even by the thermal non-equilibrium thin-film growth techniques, and larger than the 1% of tensile strain under which ferroelectricity was experimentally found, [13] though it is difficult to compare experiments and LDA-based calculations. On the other hand, Haeni *et al.* could not observe the ferroelectricity in the 0.9% compressive strained SrTiO₃ thin film on a (La,Sr)(Al,Ta)O₃ substrate. [13] It is also difficult to conclude that 0.9% compressive strain is less than the critical strain required to induce ferroelectricity or that 0.9% is enough to induce the ferroelectricity, but a surface effect (or any other effects) suppresses it.

To clarify the structural effects of in-plane biaxial strain, we analyze the detailed behavior of atomic displacements for 4% biaxial compressive and tensile strains:

Predicted results for the compressive strain, as functions of u_z , are plotted in Fig. 7: (a) total energy; (b) lattice constants; (c) and (d) atomic displacements. Ferroelectric tetragonal equilibrium, with a 40.2 meV stabilization energy gain, is predicted at $u_z = 0.456\text{ Bohr}$. The lattice constant $c(u_z)$, is well fitted with a quadratic function. Normalized atomic displacements v_z^{τ}/u_z change greatly in the investigated range of u_z , in contrast with BaTiO₃ in which they remain almost constant to the Γ_{15} soft-mode eigenvector in ferroelectric distortion [16]. In the atomic displacements of the positive charge, we can find that the displacement of Ti is dominant from paraelectric $u_z = 0$ state to $u_z = 0.456$ at

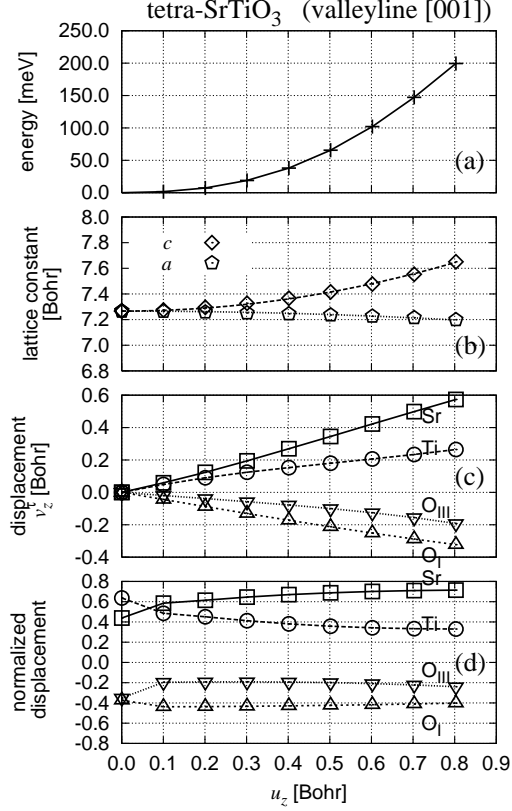


Figure 3: Calculated results for free-standing SrTiO₃ regarding atomic displacements of tetragonal [001] direction. (a) Calculated total energy (in meV) as a function of u_z (in Bohr) (+'s connected with solid lines). Zero of the energy scale is placed at the total energy of the cubic structure when $u_z = 0$. (b) Lattice constants a and c in Bohr as functions of u_z fitted by quadratic functions drawn with a dotted line and a dashed line, respectively. (c) Atomic displacements $v_z^{\text{Sr}}, v_z^{\text{Ti}}, v_z^{\text{O}_I} = v_z^{\text{O}_{II}}, v_z^{\text{O}_{III}}$ as functions of u_z . (d) Normalized atomic displacements v_z^i/u_z as functions of u_z . The Γ_{15} soft-mode eigenvector calculated by the frozen phonon method is additionally shown at $u_z = 0$.

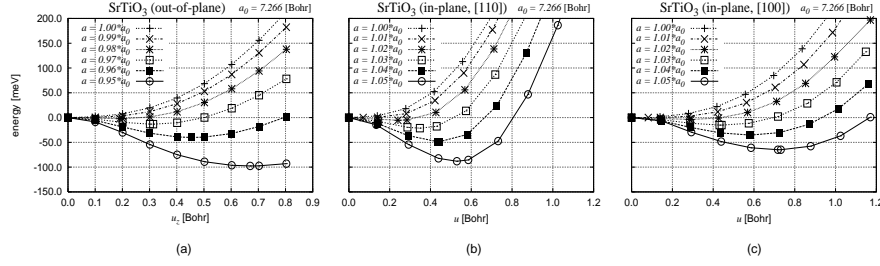


Figure 4: Calculated total energies (in meV) of SrTiO_3 as functions of $u = \sqrt{u_x^2 + u_y^2 + u_z^2}$ (in Bohr) for the tetragonal [001] distortion under in-plane biaxial compressive strains (a) and the monoclinic [110] (b) and [100] (c) distortions under in-plane biaxial tensile strains. Zero of the energy scale is placed at the total energy of the paraelectric structure (i.e., $u = 0$) for each strain.

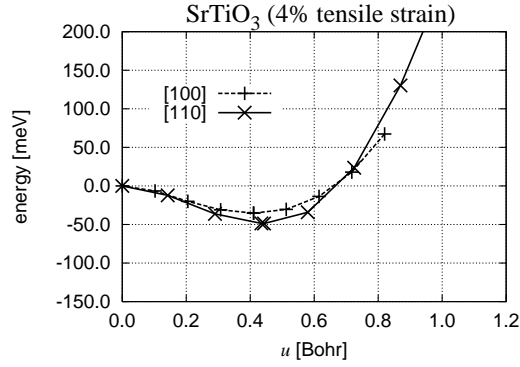


Figure 5: Comparison of u -dependence of total energies (in meV) for the monoclinic [110] and [100] ferroelectric distortions under same biaxial tensile strain of 4%.

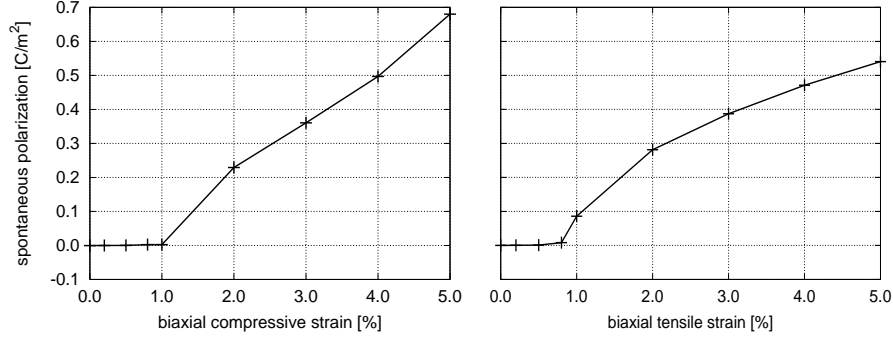


Figure 6: Calculated spontaneous polarizations of the equilibrium structures as a function of applied biaxial strains.

Table 1: Conventional atomic displacive modes. Slater mode, Last mode, and the octahedron-deformation mode. The translational mode and the Γ_{25} mode are also listed.

	Slater mode	Last mode	octa. deform. mode	trans. mode	Γ_{25} mode
A	0	$4/\sqrt{20}$	0	$1/\sqrt{5}$	0
B	$3/\sqrt{12}$	$-1/\sqrt{20}$	0	$1/\sqrt{5}$	0
O_I	$-1/\sqrt{12}$	$-1/\sqrt{20}$	$1/\sqrt{6}$	$1/\sqrt{5}$	$1/\sqrt{2}$
O_{II}	$-1/\sqrt{12}$	$-1/\sqrt{20}$	$1/\sqrt{6}$	$1/\sqrt{5}$	$-1/\sqrt{2}$
O_{III}	$-1/\sqrt{12}$	$-1/\sqrt{20}$	$-2/\sqrt{6}$	$1/\sqrt{5}$	0

which the total energy becomes minimum, whereas the displacement of Sr become activated instead of Ti in the region of $u > 0.456$, as shown in Fig.7(c). There may be a relatedness between this Sr-Ti-displacements-crossing point and the ferroelectric equilibrium structure with the minimum total energy, thus we mentioned that free-standing SrTiO_3 , which have the crossing point at around $u = 0.07$, is *very close* to having a double well. In the negative charge, the atomic displacement of $O_I (\equiv O_{II})$ is dominant compared to that of O_{III} throughout the investigated range of u_z . To obtain the deeper insights about these behavior of the atomic displacements, we analyze the presently obtained normalized atomic displacements by decomposing them into conventional three Γ_{15} modes: Slater mode, [29] Last mode, [30] and the octahedron-deformation mode, as listed in Table 1. As shown in Fig. 8, although the Slater mode is dominant through out the entire investigated range of atomic displacements, the Last mode tend to increase while the Slater mode decreases moderately as functions of the amplitude of atomic displacements u_z . This result is corresponding to the sight pointed out by Shimizu [14] and Harada [31] that the Last mode is also important while the Slater mode plays a key role in the phase transition of SrTiO_3 .

For SrTiO_3 under the 4% tensile strain, the calculated results of total energy,

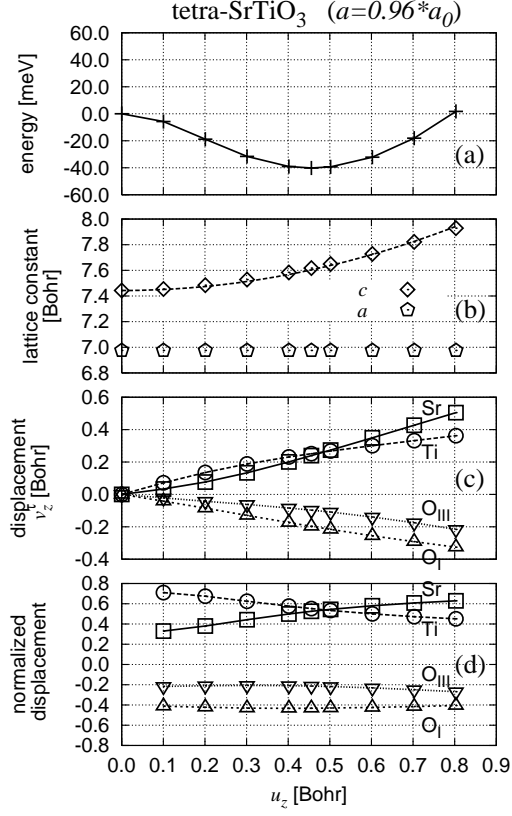


Figure 7: Calculated results for SrTiO₃ under 4% biaxial compressive strain regarding atomic displacements of tetragonal [001] direction. (a) Calculated total energy (in meV) as a function of u_z (in Bohr) (+’s connected with solid lines). Zero of the energy scale is placed at the total energy of the cubic structure when $u_z = 0$. (b) Lattice constants in Bohr. a is fixed. c is fitted by quadratic functions of u_z and drawn with a dashed line. (c) Atomic displacements $v_z^{\text{Sr}}, v_z^{\text{Ti}}, v_z^{\text{O}_I} = v_z^{\text{O}_{II}}, v_z^{\text{O}_{III}}$ as functions of u_z . (d) Normalized atomic displacements v_z^T/u_z as functions of u_z .

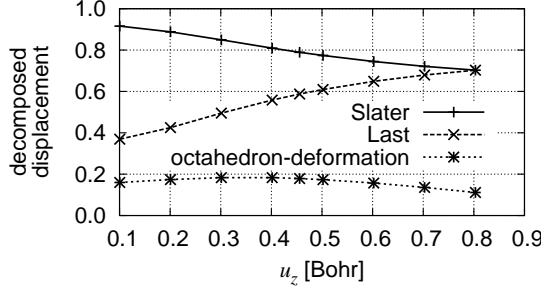


Figure 8: Normalized atomic displacements of tetragonal SrTiO_3 are decomposed into three conventional modes: Slater mode (solid line), Last mode (dashed line), and the octahedron-deformation mode (dotted line) as functions of u_z in Bohr.

lattice constants and atomic displacements of x -direction as functions of the amplitude of atomic displacements $u = \sqrt{u_x^2 + u_y^2}$ are shown in Fig. 9. In this case, ferroelectric monoclinic equilibrium structure is produced by getting the 48.6 meV energy gain at $u = 0.443$ Bohr. In the atomic displacements of the x -direction, Ti in the positive charge and O_I ($\equiv \text{O}_\text{II}$ of y -direction) and O_III in the negative charge are dominant from paraelectric $u = 0$ state to $u = 0.443$ at which the total energy becomes minimum, whereas the x -direction displacements of Sr and O_II ($\equiv y$ -direction of O_I) become active in the region of $u > 0.443$, as shown in Fig.9(c). While lattice constant c decreases slightly at first, it changes into the tendency to increase when the relation of the displacements of x -direction between O_I and O_II is reversed. We analyze the charge density distribution at each amplitude of atomic displacements u for the tensile strained SrTiO_3 . Shown in Fig.10 are the pseudo valence charge density maps in the (001) cross sections and a projection at the following three points; [A] paraelectric state at $u = 0$, [B] monoclinic equilibrium state at $u = 0.443$ Bohr, and [C] large displacement state at $u = 0.870$ Bohr, which are printed on total-energy surface shown in Fig.9(a). In the process from the paraelectric state to the monoclinic equilibrium state, we can find that Ti comes close to O_I and O_II while Sr and O_III approach mutually, shown in Fig.10[A],[B]. In other words, the closenesses of Ti- $\text{O}_\text{I}, \text{O}_\text{II}$ and that of Sr- O_III play the dominant role for ferroelectric structural distortion in SrTiO_3 induced 4% tensile strain. In the region of the large amplitude of atomic displacements $u > 0.443$, however, the displacements which O_I and O_II come close to Sr are enhanced while the closenesses of Ti- $\text{O}_\text{I}, \text{O}_\text{II}$ and that of Sr- O_III are saturated respectively, as shown in Fig.9(c) and Fig.10[C]. From these results, the displacements of O_I and O_II are shifted in the direction in which they approach Sr because the Ti- $\text{O}_\text{I}, \text{O}_\text{II}$ closeness displacement is saturated by the rigid-sphere-like ionic repulsion between them, so in the atomic displacements of x -direction in $u > 0.443$ as shown in Fig.9(c), Sr in the positive charge and O_II in the negative charge are displaced dominantly. The increase of lattice constant c works to relax the rapid closeness of Sr- $\text{O}_\text{I}, \text{O}_\text{II}$. Hence, SrTiO_3 can

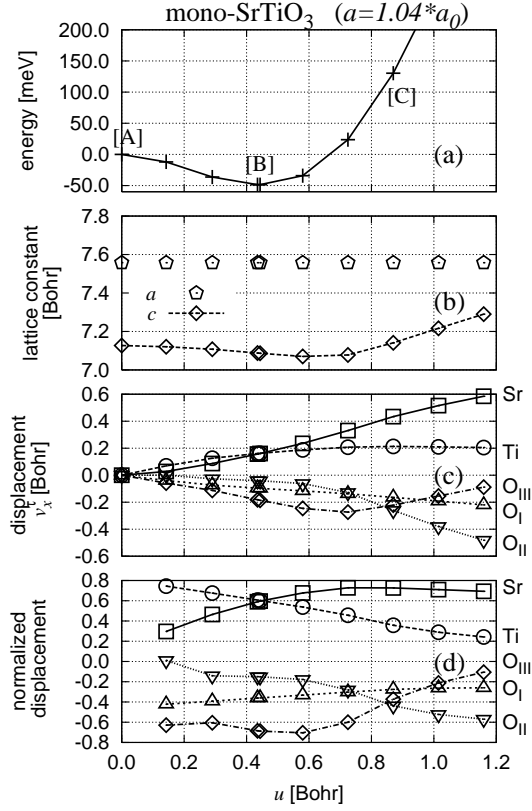


Figure 9: Calculated results for SrTiO₃ under 4% biaxial tensile strain regarding atomic displacements of tetragonal [110] direction. (a) Total energy (in meV) as a function of u (in Bohr) (+'s connected with solid lines). Zero of the energy scale is placed at the total energy of the cubic structure when $u = 0$. (b) Lattice constants c and fixed a in Bohr. (c) Atomic displacements v_x^τ . (d) Normalized atomic displacements v_x^τ / u_x as functions of u .

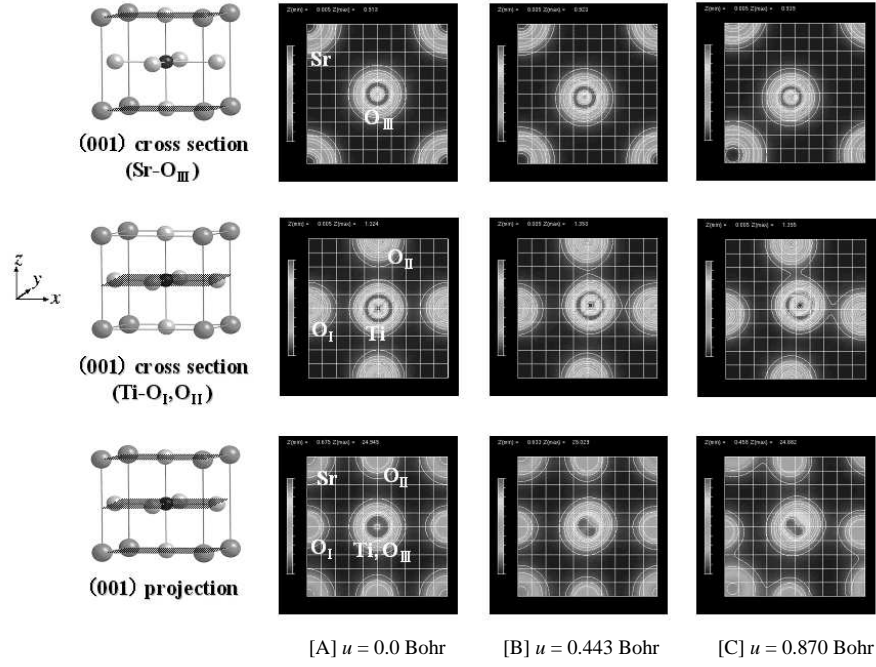


Figure 10: Pseudo valence charge density maps in the (001) cross sections and a projection for SrTiO_3 under 4% biaxial tensile strain at the following three points of atomic distortion; [A] paraelectric state at $u = 0$, [B] monoclinic equilibrium state at $u = 0.443$ Bohr, and [C] large displacement state at $u = 0.870$ Bohr, which are indicated on total-energy surface shown in Fig.9(a). Maps were drawn with VENUS. [32]

be regarded as a typical ionic crystal. The origin of the ferroelectricity can be considered that the rigid-sphere-like ions go into open spaces induced by the biaxial tensile strain.

4 Summary

In this study, we investigated the effect of the in-plane biaxial compressive and tensile strains of SrTiO_3 on the ferroelectric distortion by determining the total-energy surface accurately with our structure optimization technique. (a) We confirmed that the ferroelectric distortion is induced strongly and Curie temperature is raised by applying the biaxial compressive or tensile strains to SrTiO_3 . (b) From the results of the normalized atomic displacements, it is clarified that the ferroelectric distortion of SrTiO_3 is strongly influenced by the atomic displacements corresponding to the hard mode as well as the soft mode. (c) By analyzing the obtained normalized displacements for 4% biaxial compressive strain, we showed that the Slater mode plays a dominant role while the Last mode is also important in the ferroelectric phase transition of SrTiO_3 . (d) The behavior of atomic displacement associated with ferroelectric distortion was clarified by analyzing the charge density distribution in each amplitude of atomic displacements for 4% biaxial tensile strain.

Acknowledgements

Computational resources were provided by the Center for Computational Materials Science, Institute for Materials Research (CCMS-IMR), Tohoku University. We thank the staff at CCMS-IMR for their constant effort.

References

- [1] V. M. Goldschmidt: Akad. Oslo Math-Natur. **2** (1926) 7.
- [2] R. D. Shannon: Acta Cryst. A **32** (1976) 751.
- [3] K.-H. Hellwege and A. M. Hellwege: *Landolt-Börnstein: Numerical Data and Functional Relationships in Science and Technology* (Springer, Berlin, 1981) Vol. 16a, pp. 59–64, New Series, Group III, Vol. 16a, pp.59-64.
- [4] H. Unoki and T. Sakudo: J. Phys. Soc. Jpn. **23** (1967) 546.
- [5] P. A. Fleury, J. F. Scott and J. M. Worlock: Phys. Rev. Lett. **21** (1968) 16.
- [6] G. Shirane and Y. Yamada: Phys. Rev. **177** (1969) 858.
- [7] B. Okai and J. Yoshimoto: J. Phys. Soc. Jpn. **39** (1975) 162.
- [8] K. A. Müller and H. Burkard: Phys. Rev. Lett. **26** (1970) 13.
- [9] R. Viana, P. Lunkheimer, J. Hemberger, R. Bohmer and A. Loidl: Phys. Rev. B **50** (1994) 601.

- [10] M. Itoh, R. Wang, Y. Inaguma, T. Yamaguchi, Y. J. Shan and T. Nakamura: Phys. Rev. Lett. **82** (1999) 3540.
- [11] J. H. Barrett: Phys. Rev. **86** (1952) 118.
- [12] E. Sawaguchi, A. Kikuchi and Y. Kadera: J. Phys. Soc. Jpn. **18** (1963) 459.
- [13] J. H. Haeni, P. Irvin, W. Chang, R. Uecker, P. Reiche, Y. L. Li, S. Choudhury, W. Tian, M. E. Hawley, B. Craigo, A. K. Tagantsev, X. Q. Pan, S. K. Streiffer, L. Q. Chen, S. W. Kirchoefer, J. Levy and D. G. Schlom: Nature **430** (2004) 758.
- [14] T. Schimizu: Solid State Commun. **102** (1997) 523.
- [15] A. Antons, J. B. Neaton, K. M. Rabe and D. Vanderbilt: Phys. Rev. B **71** (2005) 024102.
- [16] T. Hashimoto, T. Nishimatsu, H. Mizuseki, Y. Kawazoe, A. Sasaki and Y. Ikeda: Jpn. J. Appl. Phys. **43** (2004) 6785.
- [17] R. D. King-Smith and D. Vanderbilt: Phys. Rev. B **49** (1994) 5828.
- [18] X. Gonze, J.-M. Beuken, R. Caracas, F. Detraux, M. Fuchs, G.-M. Rignanese, L. Sindic, M. Verstraete, G. Zerah, F. Jollet, M. Torrent, A. Roy, M. Mikami, P. Ghosez, J.-Y. Raty and D. C. Allan: Comput. Mater. Sci. **25** (2002) 478.
- [19] M. Teter: Phys. Rev. B **48** (1993) 5031.
- [20] M. Bernasconi, G. L. Chiarotti, P. Focher, S. Scandolo, E. Tosatti and M. Parrinello: J. Phys. Chem. Solids **56** (1995) 501.
- [21] S. Goedecker, M. Teter and J. Hutter: Phys. Rev. B **54** (1996) 1703.
- [22] D. M. Ceperley and B. J. Alder: Phys. Rev. Lett. **45** (1980) 566.
- [23] A. Okazaki and M. Kawaminami: Mater. Res. Bull. **8** (1973) 545.
- [24] R. E. Cohen: Nature **358** (1992) 136.
- [25] R. D. King-Smith and D. Vanderbilt: Phys. Rev. B **47** (1993) 1651.
- [26] R. Resta: Rev. Mod. Phys. **66** (1994) 899.
- [27] E. Sawaguchi, A. Kikuchi and Y. Kadera: J. Phys. Soc. Jpn. **17** (1962) 1666.
- [28] N. Sai and D. Vanderbilt: Phys. Rev. B **62** (2000) 13942.
- [29] J. C. Slater: Phys. Rev. **78** (1950) 748.
- [30] J. T. Last: Phys. Rev. **105** (1957) 1740.
- [31] J. Harada, J. D. Axe and G. Shirane: Acta Crystallogr. Sect. A **A 26** (1970) 608.
- [32] F. Izumi: J. Crystallogr. Soc. Jpn. **44** (2002) 380 [in Japanese].